HHS Public Access

Author manuscript

J Anal Toxicol. Author manuscript; available in PMC 2021 April 14.

Published in final edited form as:

J Anal Toxicol. 2021 April 12; 45(4): 337–347. doi:10.1093/jat/bkaa088.

Toxic Metal-Containing Particles in Aerosols from Pod-Type Electronic Cigarettes

R. Steven Pappas, PhD[1], **Naudia Gray**[1], **Mary Halstead**[2], **Liza Valentin-Blasini, PhD**[1], **Clifford Watson, PhD**[1]

[1]Centers for Disease Control and Prevention, Tobacco and Volatiles Branch, 4770 Buford Hwy, M.S. S110-4, Atlanta, Georgia, 30341, USA.

[2]Battelle Analytical Services, 2987 Clairmont Road, Suite 450, Atlanta, GA 30329, USA.

Abstract

The popularity of electronic cigarettes (electronic nicotine delivery systems or ENDS) has grown rapidly over the past decade. With the continued evolution of ENDS, and the arrival of newer replaceable pod devices on the market, it is prudent to examine their emissions to help determine potential health risks to the user. Metal containing particles were examined in aerosol from several pod-based devices from three manufacturers that offer flavored liquids in their respective products.

Previous ENDS metal emissions studies focused on the total toxic metal concentrations in aerosols and have suggested that the principal sources are oxidized internal metal components that are in contact with the liquid. Most metal oxides have limited solubility and it is likely that some metal content in ENDS aerosol may present as particles rather than dissolved forms. Examining the composition and number of particles in the ENDS aerosols is important because inhaled metal oxide particles cause pulmonary inflammation. Chronic inhalation of ENDS aerosol may lead to inflammatory cell activation in the lungs. Therefore, this study was designed to measure metal oxide particle concentrations and sizes in ENDS aerosols from select pod-based systems.

Aerosol samples were generated with pod liquids (tobacco, mint or menthol) from devices produced by three manufacturers using CORESTA Recommended Method 81 parameters with a high purity fluoropolymer aerosol trap. Particle sizes for chromium, iron, nickel, copper, zinc, tin, and lead oxides were measured in triplicate using Single Particle-Inductively Coupled Plasma-Mass Spectrometry and Dynamic Light Scattering. A novel aspect of these measurements included using dual element particle analysis to infer particle source component material. Particle concentrations in aerosols from the devices were variable between devices and from pod to pod, ranging from no detectable chromium and zinc containing particles in aerosol from some pods to 222,000 lead containing particles per 10 puffs from individual pods.

Corresponding Author: RPappas@cdc.gov.

Introduction

Electronic cigarettes (electronic nicotine delivery systems, ENDS) have become the most commonly used tobacco product among adolescents (1,2). There are many different types of electronic cigarettes, including cig-a-likes, pen-type devices, pods, and mods. The most recent ENDS devices on the market are designed with replaceable pods. The replaceable "pods" contain the liquid solvent (propylene glycol, glycerol, and water), nicotine, the heating element, the vapor tube, and battery connections. The heating element is often comprised of metal and may be in the form of a metal coil. Metal can also be present in the battery connections which can be partially exposed to the liquid and in the material used to join battery connections, and the heating element. These ENDS components are often constructed of stainless steel (chromium, iron, nickel, manganese), nichrome (nickel, chromium), brass (copper, zinc), kanthal (aluminum, chromium, iron) or, tin-lead solder.

When determining toxicant emissions in ENDS aerosol, a detailed description of puff regimen and aerosol generation and capture is essential so that data obtained by different laboratories may have sufficient parity to provide results that are comparable and generalizable. Aerosol sample collection and preparation containers used for quantitating metal content should be made from high purity materials such as polypropylene, polymethylpentene (PMP), or fluoropolymers where leachable metals do not contaminate the sample, as is the case for all glassware, glass fiber filters, and low purity quartz filters. The concentrations of chromium, nickel, copper, zinc, cadmium, tin, and lead in aerosol obtained from early to recent generation ENDS devices using the CORESTA Recommended Method 81 puff regimen and collected using a high purity fluoropolymer trap have been reported (3). Metal particles from the ENDS aerosol were analyzed in this study using single particle inductively coupled plasma-mass spectrometry (SP-ICP-MS) and Dynamic Light Scattering (DLS). Recent SP-ICP-MS software developments and faster electronics have enabled concurrent dual element analysis in individual particles. If particles consisted of multiple metal oxides, but only single elements were sequentially analyzed, it is possible that total particle mass and size would be underestimated based on the assumption of a single metal oxide in each particle. Therefore, both single and dual element analyses were performed on aerosols from a subset of pod-type ENDS devices in order to determine whether the particles consisted of individual metal oxides or multiple metal oxides. Juul® Mint and Classic Tobacco, myblu® Mint-sation and Tobacco Chill, and Vuse Alto® Menthol and Rich Tobacco were analyzed for chromium, iron, nickel, copper, zinc, tin, and lead containing particles and chromium-iron, chromium-nickel, iron-nickel, and copper-zinc dual analyte containing particles.

Materials and Methods

Reference material and manufactured nanopowder preparation for method validation

Nanoexact gold nanospheres (31 nm mean stated size, 1.8×10^{11} particles/mL, Nanocomposix, San Diego, CA, USA) were used for calibration of particle transport efficiencies on the basis of particle concentration after $1{:}5{\times}10^{6}$ dilution to a calculated concentration of 36,000 particles/mL. In addition, they served as the particle size standard for particle size calibration together with 1.00, 2.00, 3.00, and 4.00 μg/L dissolved gold

standards prepared by dilution of a NIST-traceable 1000 μg/mL standard (High Purity Standards, Charleston, SC, USA). The diluted particles were also analyzed in triplicate as samples on separate analytical run days for validation purposes.

NIST Standard Reference Material 1898 Titanium Dioxide nanomaterial (NIST, Gaithersburg, MD, USA) was prepared at 1.0 mg nanopowder per mL ultrapure water, within the concentration range validated for sonication by NIST, prior to sonication (4). Sonication was performed similarly to the procedure described in the certificate (4). Nanomaterial was suspended using a QSonica 125 sonicator with a 15 minute sonication time in a 2-propanol/ice bath as described in the NIST procedure. The same 8 seconds on, 2 seconds off duty cycle described in the NIST procedure was used, but a 6 mm diameter sonicator horn was used with a 10 mL suspension volume instead of a 1.27 cm horn with a 50 mL suspension. At 100% amplitude, this sonicator/horn combination provided approximately 20% power to the suspension (after subtraction of the power delivered to air), or 25 Watts delivered to the 10 mL suspension (2.5 Watts per mL, compared to 1.0 Watt per mL in the larger volume NIST procedure). After sonication, the 1 mg/mL suspension was immediately serially diluted 1/100 with vortexing to a final $1:10^6$ dilution in ultrapure water for SP-ICP-MS analysis or 1:100 for DLS analysis. New sample preparations were performed for triplicate independent analyses on different analytical run days.

U.S. Research Nanomaterials (Houston, TX, USA) and Nanoshel manufactured nanopowders (Wilmington, DE, USA) described in the SP-ICP-MS Instrumentation section were used to prepare 1.0 mg/mL, 10 mL suspensions in ultrapure water and sonicated with the same horn probe, duty cycle and power settings as described for NIST TiO_2. The suspensions were sonicated for 1, 5, 10, 15, and 30 minutes, then immediately serially diluted 1:100 with vortexing to a final dilution of $1:10^6$ for analysis with SP-ICP-MS to determine optimum sonication times. Though particle diameters of these materials are not certified, images of the individual materials obtained using transmission electron microscopy are available on the respective manufacturers' web sites.

Sample collection and preparation for analysis

Pod-type ENDS devices and pods are trademarks of respective manufacturers and were obtained from vendors in the greater Atlanta, GA USA area or via the internet. Three brands with two flavors each were chosen for this study based on popularity and availability: Juul® Mint and Classic Tobacco, myblu® Mint-sation and Tobacco Chill, and Vuse Alto® Menthol and Rich Tobacco. Physical characteristics of these pods include an iron, chromium, and nickel alloy coil (8.5 W, 1.6 ohm) with silica wick, (Juul®), nichrome coil (10.5 W, 1.3 ohm) with cotton wick (mblu®), and 6.5 W with 1.1 ohm porous silicate block (Vuse®).

Aerosols were generated using a Cerulean (Richmond, VA, USA) CETI-8 e-cigarette aerosol machine. Condensed aerosol was collected from unused pods with freshly charged batteries for each replicate analytical run. Aerosol (75 puffs) was generated using CORESTA Recommended Method 81 puff parameters: 55 mL puff volume, 3 second puff duration, rectangular puff profile, 30 second puff interval (5). Puff volume accuracies were verified daily using calibrated soap bubble meters. Each tubing trap was tested to assure that puff

profiles met CORESTA Method 81 specifications and to ensure puff consistency. This is necessary because any elevated pressure drop could impact the puff profile and could delay activation of the ENDS heating elements. The aerosols condensed inside previously described (3) ultrapure acid cleaned fluorinated ethylene propylene (FEP) tubing traps (Savillex, Eden Prairie, MN, USA). The condensate was rinsed from the trap with three 8 mL ultrapure water flushes. Samples were brought to 25.0 mL total volume with ultrapure water in acid cleaned polymethylpentene (PMP) class A volumetric flasks. Particle concentrations were multiplied by final analytical volume (25.0 mL) and divided by 7.5 to convert results from particles per mL·75 puffs to particles per 10 puffs, a puff number in the intermediate range among U.S. cigarettes smoked using WHO intense smoking regimen (6). ENDS aerosol procedural condensation tube rinse blanks were used in each analytical run to assure no false positive particle results. Condensation tubes were repeatedly rinsed after each aerosol collection with 1% v/v hydrochloric acid + 1% v/v nitric acid, ultrapure water, and dried prior to subsequent use. Aerosol collections and analyses were performed on three different days, and the triplicate average results are reported.

DLS Standard Reference Material (SRM) and aerosol analysis

After rinsing aerosol from condensation tubes, samples were directly analyzed using a Malvern Zetasizer NSP Dynamic Light Scattering instrument (Malvern Panalytical, Westborough, MA, USA) with detection of 173° backscattered light from the 10 mW He-Ne 632.8 nm incident laser at 25.0°C without further preparation. The 2.41 refractive index for TiO2 at 633 nm was obtained from a table of select materials in a Malvern instrument blog (13). Since DLS is not elementally specific, the 2.630 refractive index for copper(II) oxide at 633 nm obtained from the Malvern sample dispersion and refractive index list (7, 8) was chosen due to the consistent presence of sufficient copper-containing particles for analysis in all ENDS aerosol samples tested using SP-ICP-MS.

SP-ICP-MS instrumentation

SP-ICP-MS analyses were performed using two Nexion 300D instruments (PerkinElmer, Shelton, CT, USA) with Elemental Scientific (ESI, Omaha, NE, USA) Peltier-cooled spray chambers and PFA-HS nebulizers for high transport efficiency while preventing nebulizer clogging. Liquid flow rates were determined daily and were typically 375 to 400 microliters/minute (20 rpm peristaltic pump speed with 0.44 mm i.d. tubing). Instruments were optimized for highest signal while maintaining $^{140}Ce^{++}$ and $^{140}CeO^{+}$ below 2.5% and 2.0%, respectively, to minimize analytical interferences. Premium grade 99.9995% purity ammonia (Airgas, Chamblee, GA, USA) was used in cell gas modes.

Software for SP-ICP-MS particle analysis was Syngistix version 2.5, build 1811.44 with beta version Nano Analysis module 3.0, which enabled dual element as well as single element particle analysis. Particle analyses were performed using 50 μs dwell times, 100 second sample analysis times. Cell optimization parameters in Table 1 were used with default Syngistix RPq settings in single and dual element particle modes. Dual element pairs were chosen based on the possibility of particle origin from nickel-chromium alloys, stainless steel, brass, or tin-lead solder. Quadrupole settle times are “0” in single element particle mode, but optimization was required (Table 1) for dual element particle mode. The

combinations of cell gas flow and axial field voltage required to produce particle ion plume peak width durations greater than 2000 μs for sufficient data points across the peaks in dual element mode were determined using sonicated Cr_2O_3, Fe_2O_3, Ni_2O_3, CuO, ZnO, and SnO_2 metal oxide suspensions prepared from US Research Nanomaterials and Nanoshel Pb_2O_3 nanopowders described in Table 3. With ion plume durations greater than 2000 μs, 50 μs dwell times for each of two isotopes resulted in a minimum of 20 sampling points across each isotopic peak.

Particle concentration calibrations were used to determine transport efficiencies. Calibration standards for SP-ICP-MS were prepared by dilution of NIST traceable single element Au, Ti, Cr, Fe, Ni, Cu, Zn, Sn, Pb 1000 μg/mL standards obtained from High Purity Standards in 1% v/v hydrochloric acid + 1% v/v nitric acid + trace hydrofluoric acid. The stock acid solution used to prepare the standards served as calibration blanks. The calibration ranges for four multielement standards were from 1.00 to 25.0 μg/L chromium, iron, nickel, copper, zinc, tin, and lead, the principal materials from which ENDS devices are constructed. The calibration range for titanium standards was 1.00 to 10.0 μg/L.

Microscopy instrumentation and conditions

The analyses of internal components of ENDS devices were acquired with a Quanta 250 Field Emission Gun Scanning Electron Microscope (SEM) (Thermo-FEI Co., Hillsboro, OR, USA). Images were acquired in high vacuum mode (20kV) using the Everhart Thornley detector. The SEM was equipped with an Energy Dispersive X-Ray (EDS) attachment with an 80 mm^2 X-Max^N Silicon Drift Detector (SDD) (Oxford Instruments, Concord, MA, USA with Aztec software.

Light microscopy was performed using an Olympus (Center Valley, PA, USA) SZX16 stereo microscope with transmitted light base, DP73 camera, Cellsense operating system and Fostec illuminator.

Results and Discussion

Validation: Gold and sonicated metal oxide particles

The use of Standard and Certified Reference Materials (CRM) with established certified values is fundamental to method validation. However when there are no established methods for a particular matrix or reference materials with certified values for a given property or analyte, SRM reference values may be substituted along with comparisons to results obtained using other methods or instrumentation (9). Gold nanospheres (31 nm) were used to determine particle transport efficiencies. Transport efficiencies were typically between 4% and 4.5%, which falls within the upper end of typical transport efficiencies (1% to 5%) described by Pace et al. (10), likely due to the use of a Peltier-cooled introduction system. However, the diluted suspensions were also analyzed as samples for validation purposes. Most frequent sizes (particle size peaks) matched the certificate within acceptable limits (Table 2) with only slight run day to run day variability when dilutions were freshly prepared. Mean sizes differed less than 1 nm from most frequent sizes (Table 2) due to slightly asymmetric particle distributions. Mean particle counts per mL resulting from

particle concentration calibration were within 3% of the expected result calculated based on serial dilution (Table 2). Particle number concentrations resulting from particle size calibration are frequently inaccurate (11) in the absence of an appropriate internal standard, which the current state of software development does not permit.

Although the NIST SRM 1898 Titanium Dioxide nanopowder is not certified for particle size, the mean size results obtained using SP-ICP-MS after sonication compared favorably with mean particle information results obtained using Laser Diffraction Spectrometry and Laser Disk Centrifugation after the sonication procedure described in the certificate (Table 3). Although the power applied per unit volume in sample analyses reported here was greater than applied with the horn and power combination described in the NIST certificate (4), the use of greater power than necessary to disaggregate TiO_2 particles has not been shown to further improve aggregate reduction (12). The SP-ICP-MS mean result for analysis of NIST Titanium Dioxide Nanopowder also fell within the 70 – 81 nm size range calculated if measured using Laser Diffraction Spectrometry (13). The mean results obtained using DLS that were reported by one lab in the NIST certificate (4, Table 3) fell slightly below the calculated and expected 120 – 127 nm mean range for that technique, whereas our mean DLS results were within the calculated D90 143 – 163 nm range, but above the calculated mean range (Table 3). DLS analysis of 1/10 and 1/500 dilutions of the sonicated particles gave slightly higher mean results. The 1/100 dilution was therefore appropriate and was approximately the same dilution used for the DLS results in the NIST certificate.One possible reason for this difference is that large particles in a broad particle size population scatter more light than small particles (14) and may have biased the sensitivity for particle size distribution measurement in favor of larger particles if our sonicated particle size distribution was larger than the preparation used for the DLS results reported in the NIST certificate. SP-ICP-MS results for the sonicated particles, however, were very close to results reported for the other two techniques (4).

Nanopowder preparations from US Research (USR) and Nanoshel (NS) are not certified for particle size, but the manufacturers state mean sizes for each product based on particle size counts in images obtained using Transmission Electron Microscopy. TEM images for each product may be viewed on the respective manufacturers' web sites (citation 15, and respectively for each product). Visual inspection of the TEM images frequently show agglomerated individual particles rather than images of discrete particles. Nevertheless, the use of appropriate sonication times up to 30 minutes for individual nanopowders provided SP-ICP-MS most frequent size or mean size results that were very close to stated product particle sizes with few exceptions (Table 4). For example, 30-minute sonication times were required for USR Cr_2O_3 and Fe_2O_3. The most frequent sizes (size distribution peaks) determined for Cr_2O_3 and Fe_2O_3 were 60 nm and 23 nm, respectively. Our measurements matched those stated by the manufacturer (Cr_2O_3) or were within the manufacturer's stated 20 to 40 nm range (Fe_2O_3). The Cr_2O_3 and Fe_2O_3 mean sizes were higher than the most frequent sizes (Table 4), due to asymmetric particle size distributions. The particle counts for both Cr_2O_3 and Fe_2O_3 were still increasing at 30 minutes. These data indicated that still longer sonication times may have been optimum for these two nanopowders and that decreased distribution asymmetry might have resulted from sonication times beyond 30

minutes. Extended sonication times were not attempted in order to avoid accelerated instrument component wear or damage, per manufacturer's instructions.

The mean particle number for Ni_2O_3 reached a maximum after 10 minutes sonication time, but both the most frequent and mean particle sizes determined using SP-ICP-MS were lower than the size stated by the manufacturer. The manufacturer's product TEM image shows a wider size distribution for Ni_2O_3 than for Cr_2O_3 and Fe_2O_3 nanopowders with apparently a greater number of smaller particles than larger particles (15). After sonication for 10 minutes, the apparent Ni_2O_3 particle sizes leveled off, but particle number began to decrease with sonication time, possibly due to reaggregation, since dissolution was minimal. The particle size detection limit was higher for Ni_2O_3 than for Cr_2O_3 and Fe_2O_3, likely due to using the less abundant ^{60}Ni isotope in order to avoid interference from ^{58}Fe on ^{58}Ni.

The mean particle number for CuO remained relatively constant after 10 minutes sonication time. The most frequent 33 nm CuO particle size determined by SP-ICP-MS was within the 25–55 nm size range stated by the manufacturer. The mean sizes were higher than the most frequent sizes (Table 4), however, due to asymmetric particle size distributions as described for Cr_2O_3 and Fe_2O_3.

The mean particle counts for ZnO were low relative to the other metal oxides but increased up to a 10-minute sonication time before decreasing. The most frequent and mean particle sizes increased up to 15-minute sonication time, after which the sizes decreased. The dissolved ^{66}Zn background intensity increased with sonication time, beginning at 1 minute. Taken together, this likely indicated initial dissociation of particle agglomerates into a greater number of smaller "soft agglomerates" (physical attraction) that were subsequently converted to "hard" chemically bonded agglomerates (14), or more likely, due to dissolution, as has been reported for zinc oxide particles (16). The dissolved background intensity was likely the reason for the somewhat higher particle detection limit for ZnO, as well as for irregular threshold problems later encountered during dual element particle analysis (Table 6).

At 1-minute sonication time, the most frequent Pb_2O_3 particle size was 28 nm, within the manufacturer's stated range. The mean particle size at 1 minute was greater than the stated size range due to asymmetric particle size distribution. The particle number for Pb_2O_3 declined for all sonication times beyond 1 minute, as particle detection limits increased due to dissolved background. The most frequent and mean particle sizes also increased between 1- and 15-minute sonication times before decreasing at 30 minutes, as was the case for ZnO. This likely indicated initial dissociation of particle agglomerates, after which dissolution increased, or perhaps loss of small particles to fewer "hard agglomerates," similarly to ZnO (12).

At 10 minutes sonication time, the mean most frequent SnO_2 particle size was 35 nm, within the manufacturer's stated size range. The mean particle size reached a maximum of 52 nm at 10 minutes, also within the manufacturer's stated size range. After sonication times longer than 10 minutes, both the most frequent and mean particle sizes began to decline, while the mean particle number for SnO_2 increased. This likely indicated either ongoing dissociation

of particle agglomerates, after which a smaller particle population was produced, or perhaps gradual particle dissolution.

With the exception of ZnO, nanopowder particle sizes agreed well with the manufacturers' stated sizes when optimally sonicated. Although Ni_2O_3 frequent or mean sizes differed from the manufacturer's stated size, the manufacturer's TEM image showed very dispersed particle size (15); and the mean and most frequent sizes determined using SP-ICP-MS were likely consistent with the more numerous small to medium particle population in that case.

Intermediate precision was calculated as relative standard deviation of mean particle size for each metal oxide in Table 4. The metal oxide particle results that exhibited the least precision were Ni_2O_3, for which the manufacturer's TEM image showed a wide variety of particle sizes, ZnO, for which particle sizes increased up to 10 minutes sonication time before decreasing as particle number increased up to 10 minutes before decreasing while median and mean particle sizes increased up to 15 minutes before decreasing. Since dissolved zinc background increased, this likely indicated particle dissolution (16), and Pb_2O_3, which exhibited similar behavior.

ENDS aerosol particle analyses

Particle results from mint, menthol and tobacco flavored ENDS aerosols obtained from pod devices were obtained (Table 5). Particle Detection Limits (PDL) differed between triplicate analytical runs by two nm or less for most samples, therefore only mean PDLs are shown in Table 5 unless triplicate runs had wide PDL ranges. The number of particles delivered per 10 CORESTA regimen aerosol puffs differed widely from pod to pod, so the ranges of particle concentrations are shown in Table 5 rather than mean values as well. Total metal concentrations determined in aerosol from separate groups of pods from the same manufacturers (17), also reflected diverse concentrations of some metals from pod to pod, which confirmed the commonly observed variability of metal or particle concentration even among pods purchased at the same time.

In most cases, the differences in most frequent size (from the particle size distribution peak) and mean particle size from the ENDS aerosol were smaller (Table 5) than the differences in nanoparticle frequent and mean sizes from the manufactured suspensions of nanopowders (Table 4). This is possibly due to the difference in particle origins in manufacturing processes versus aerosol particle origins as ENDS device components corrode. There were few detectable chromium-containing particles per 10 aerosol puffs from myblu Mint-sation®, Juul Mint®, and only slightly more in aerosol from Juul Classic Tobacco®, myblu Tobacco Chill®, Vuse Alto Menthol®, and Rich Tobacco® pods. These data are consistent with total aerosol chromium concentrations reported as below the method LOD for newer Juul pods (3). Zinc oxide particle concentrations per 10 puffs were also low. Low zinc concentrations were predominantly dissolved, rather than in particle form. Very low dissolved metal content contributed to irregular thresholds for metals such as tin and lead as well in Juul® pods. None of the pod systems evaluated had evidence of tin or lead solder. However, SEM-EDS analyses showed that some pod components had alloys that included small percentages of lead and tin (Vuse®) or small tin particle inclusions dispersed in the otherwise homogeneous alloy (myblu®), whereas tin and lead observed in aerosols from

previous generations of ENDS devices often originated from the use of solders (3). The electrical connectors for all three pod systems were composed of a nickel/gold coated alloy. The cores of the myblu® electrical connectors were found to contain low levels of tin, while the Vuse® electrical lead wire to the nickel/gold coated connector was found to contain low levels of tin and lead in the subsurface alloy. No tin or lead was observed on surface alloys of any of the electrical connectors. However, the connector was crimped onto the lead, causing cracks in the surface of the connector, allowing liquid contact with the core composition of the connector (Figure 1). This is an explanation for the presence of tin, lead, copper and zinc in the liquid and aerosol of this device. Currently, the Syngistix Nano 3.0 software is not capable of establishing a sufficient threshold for subtraction of dissolved content or other backgrounds. Attempts to manually set sufficient thresholds with the beta version of this software resulted in software crashes. Particle Detection Limits were nevertheless acceptable using an efficient particle tolerant nebulizer and Peltier-cooled spray chamber. When future versions of the software have threshold setting capabilities, whether automatic or manual, Particle Detection Limits are likely to improve even further. This needed improvement together with existing fast electronics will empower future particle analyses.

There were no detectable lead containing particles in aerosols from myblu Mint-sation® pods that were analyzed for this study, and very few in aerosol from Juul Mint®, Classic Tobacco®, and some myblu Tobacco Chill® pods. These data were consistent with aerosol lead concentrations below detection limit for all Juul® pod flavors analyzed in another study (3) and with SEM/EDS analysis of the internal metal components that were in contact with the liquid for the devices evaluated. Particle concentrations ranged from no detectable lead containing particles to 41,000 particles per 10 puffs in aerosol from a myblu Tobacco Chill® pod.

Tin containing particle concentrations ranged from very low in aerosol from most pods to 170,000 particles per 10 puffs in aerosol from myblu Tobacco Chill®, again illustrating the variability from pod to pod. The elevated number of tin particles (170,000 per 10 puffs) was observed in aerosol from one pod. SEM-EDS analysis showed that tin was not a component of the surface material but was a minor component of the cores of myblu® and Vuse® electrical connectors.

Copper oxide particles were elevated in myblu® and Vuse® pod aerosols in comparison to aerosols from Juul pods. SEM-EDS analysis showed that the cores of the electrical connectors in both myblu® were composed of approximately 95% copper and 5% tin, and interiors of the Vuse® connectors were approximately 60% copper, 30% zinc, with small amounts of iron, tin, and lead. The compositions of the cores of the Juul® electrical connectors were consistent with stainless steel. This data was consistent with the higher numbers of copper-containing particles in aerosol from myblu® and Vuse® pods compared to aerosols from Juul® pods. Further investigation of electrical connectors from myblu® pods before and after vaping 50 puffs showed development of copper-containing corrosion on the surface during vaping (Figure 2). The determination of high concentrations of copper-containing particles in aerosol obtained from some pod devices is consistent with elevated copper concentrations in total aerosol metal analyses of previous generations of Blu® and

Vuse® devices in which copper was a component of brass electrical connectors (3). However, SEM-EDS analysis of myblu® pods purchased two months later than the purchase of the pods from which aerosol was obtained for this study, revealed that the compositions of the core of the electrical connector had changed to 70% iron, 20% chromium, and 10% nickel, consistent with a stainless steel alloy.

Low concentrations of nickel and iron oxide particles were also observed in aerosol from pods from all devices. Nickel and iron particle concentrations ranged from fairly low in aerosols from all three manufacturers' pods (3), consistent with previously reported low nickel concentrations in total Juul aerosol metal analyses) to 190,000 particles per 10 puffs in aerosol from one Vuse Alto Rich Tobacco® pod. SEM-EDS analysis revealed that all manufacturers' pods had 80% to 85% nickel and 15% - 20% gold as components of the electrical connector surface alloys. Heating elements consisted of nickel and chromium (nichrome) in Juul® pods, a nickel, iron, chromium alloy in myblu® pods, but the Vuse® ceramic heating element, constructed from predominantly silicon oxides with a small amount of aluminum, contained no nickel.

Dual element particle analysis capabilities of Syngistix beta nanoparticle software module version 3.0 were explored to determine if there were evidence of particle formation that consisted of multiple metal oxides in aerosols. The dual element capabilities required the determination of a quadrupole settling time that is not used in single element particle mode, and determination of a combination of axial field voltage and cell gas flow that prolongs the time for particle ion plumes to pass through the cell. The expansion of particle ion plume time widths to 2,000 μs or greater is intended to provide a sufficient number of sampling points across the intensity peaks for each of two coincidental particle elements when the ion plumes reach the detector. Axial field voltage was decreased from optimum intensity settings in favor of expanding the particle ion plume width through the cell. This decreased sensitivity, increased particle detection limits for these analyses, and resulted in lower particle counts, while imparting the advantage of determining whether there was evidence for particles consisting multiple metal oxides. The software can overlay ion impacts on the detector that occur within the same ion plume and infer particles that have two elements. Element pairs were chosen to reflect possibilities of dual element particles resulting from corrosion of steel or kanthal (chromium/iron, iron/nickel), nichrome alloys (chromium/nickel), brass (copper/zinc), and some solders (tin/lead). Because of current instrument limitations, it was not possible to determine whether tin and lead oxides were paired in single particles. Although ammonia and heavier cell gases (nitrogen and argon) were attempted with the tin/lead element pair, there were no combinations of axial field voltage and cell gas flow that provided both sufficient analytical sensitivity at manufactured particle sizes used in this study, and peak shapes that were sufficiently wide to make such measurements.

Dual element particle analyses for the chromium/iron-containing pairs (mint or menthol flavored pods, Table 6) showed that although the total aerosol chromium-containing particle concentrations were low, and were low compared to the number of iron-containing particles, all of the chromium oxide was paired with iron oxide in aerosol from the Juul Mint® pod, consistent with the composition of the stainless steel aerosol tube, or possibly the core of the

electrical connector. Half of the chromium oxide was paired with iron oxide in aerosol from the myblu Mint-sation® pod, consistent with the composition of the steel alloy used for the aerosol tube. None of the very low numbers of chromium oxide particles were paired with iron oxide in aerosol from Vuse Alto Menthol®. This was consistent with the absence of steel or nichrome components in Vuse® pods, according to SEM-EDS analysis. Results of dual element particle analyses for the iron/nickel pair suggested that almost half of the total Juul® pod aerosol iron was paired with nickel. Approximately one in six iron-containing particles in aerosol from Vuse Alto® pods was paired with nickel, and none of the iron-containing particles in aerosol from myblu Mint-Sation® was paired with nickel. Dual element particle analyses for the chromium/nickel-containing pairs (Table 6) showed that there were no paired chromium and nickel-containing particles in aerosols from myblu® or Vuse Alto®, and 2.0% of total nickel and 20% of chromium-containing particles were paired in aerosol from the Juul pods. Stainless steel alloys range from approximately 10.5% to 26% chromium and 0% to 12% nickel (18–20). Stainless steel alloys are known to leach into foods during cooking (20), whereas nichrome, often 80% nickel and 20% chromium, is resistant to oxidation even at elevated temperatures unless in the presence of strongly oxidizing acids (21). Taken together, these data are more consistent with the possibility of steel or similar iron-containing alloys as significant sources of chromium, iron, and nickel oxide-containing particles, rather than with nichrome heating elements. These data do not support suggestions (22–24) that nichrome heating elements (or filaments) are principal sources of nickel and chromium in ENDS aerosols in recently obtained single use devices or pods used in this work, although we cannot rule out limited degradation of nichrome heating elements used for greater lengths of time in devices with refillable tanks or cartridges.

Most of the Vuse Alto® copper-containing particles were unpaired, as expected when no brass is present on the surfaces of device components. Although 43% of zinc-containing particles were determined as paired, there were very few zinc-containing particles, resulting in pairing with only 0.5% of the copper-containing particles. However, closer examination of the alloy below the surface of the connector using SEM-EDS showed that there was brass below the surface that also contained small amounts of tin and lead. Since this alloy was not on the surface where it would be exposed to the ENDS liquid, this finding is consistent with the low number of particles with paired copper and zinc in the aerosol. Thus a significant change of component design among pod devices compared to earlier generation devices is the determination of no brass components superficially exposed to liquids.

Dynamic light scattering particle analyses as copper(II) oxide

Dynamic light scattering (DLS) is selective for refractive index, but not specific for a given metal oxide. Therefore, a typically abundant oxide, copper(II) oxide, was chosen for DLS analysis although particles of other metal oxides may have been detected as well. Some of the DLS results (Vuse Alto Rich Tobacco®, myblu Tobacco Chill®, myblu Mint-sation®) agreed reasonably well with the SP-ICP-MS results, and the Vuse Alto Menthol® DLS result had some overlap in agreement with the SP-ICP-MS results. The Juul Classic Tobacco® and Juul Mint®, results noticeably differed from the SP-ICP-MS results.

The aerosols from Juul® pod flavors had a wide range of particle numbers as determined by SP-ICP-MS. If aerosol copper(II) oxide particles from the pods used for DLS analysis were at the lower end of the concentration range, it is possible that the low numbers of smaller sized particles that scatter less light were largely “overlooked” because of bias toward larger particles that scatter more light (20). This explanation is also supported by the high standard deviations observed for the DLS results for the two Juul® flavors. Two of three aerosol replicate analyses of myblu Mint-sation® were close to the SP-ICP-MS results, but one replicate was significantly lower, which decreased the mean size.

Since aerosols from many pods have low particle concentrations, and DLS does not provide the capability to count particles, it would not be possible to know when results might be biased due to lower or higher than optimum particle concentrations, unless the same sample were divided and used for side by side analyses with SP-ICP-MS. However, it was possible to see average DLS copper oxide particle size peaks gradually increasing in size with each replicate, indicating agglomeration over the analytical time frame. In order to perform side by side analyses, it would be necessary to split samples and analyze them simultaneously. The known size bias (14), the lack of specificity for a single metal oxide, a few discrepancies between results obtained using the DLS instrument and SP-ICP-MS, the discrepancy between DLS results reported in the NIST SRM 1898 certificate (12) and those reported here suggest that the SP-ICP-MS results were more reliable when the particle size results differed.

Health considerations

Previous work has shown that metal concentrations in ENDS liquids that are not in contact with metal device components were below limits of detection, whereas metal concentrations in liquids exposed to ENDS device metal components were increased with age (25). Regardless of the internal sources of metal-containing particles from oxidized components, no inhalation of metal oxide particles is beneficial to health. Although some of the particle sizes reported in Table 5 were in the fine range (100 nm to 2.5 μm), a large number of the metal oxide particles in aerosol were ultrafine (smaller than 100 nm) and were therefore incidental (not manufactured) nanoparticles formed by product degradation. Chronic inhalation of metals in particulate imparts health risks consistent with elemental composition (24, 26–29). The inhaled particle size, however, determines the depth of pulmonary particle deposition, as decreasing particle size in the ultrafine size range is associated with deeper airway penetration (30). Smaller particle size is also associated with a greater extent of alveolar interstitial particle translocation (31, 32). In summary, use of these ENDS products results in inhalation exposures to potentially harmful nanoparticles.

Conclusions

Dynamic light scattering and a new SP-ICP-MS method for the analysis of metal-containing particles derived from the internal oxidation of the new generation of ENDS pod device components was presented. The results of the analyses of NIST titanium(IV) oxide nanoparticles and other manufactured metal oxide nanoparticles using this method were in good agreement with the available informational sizes, whereas the NIST titanium(IV) oxide

results were questionable when Dynamic Light Scattering was used. Particles from pod type ENDS device aerosols were characterized on the basis of metal composition, particle size, and aerosol particle concentration. In addition, a new dual element particle analysis mode was used to determine whether particles might consist of multiple metal oxides in order to infer the particle source material. The results of paired particle analyses made possible with dual element software capabilities, provided information to make implications on likelihood of different internal device materials as possible sources of the aerosol particles.

References

1. Arrazola RA, Singh T, Corey CG, Husten CG, Neff LJ, Apelberg BJ, Bunnell RE, Choiniere CJ, King BA, Cox S, McAfee T, Caraballo RS. 2015. Tobacco use among middle and high school students - United States, 2011–2014. MMWR Morbidity Mortality Weekly Report. 64, 381–385. [PubMed: 25879896]
2. Gentzke AS, Creamer M, Cullen KA, Ambrose BK, Willis G, Jamal A, King BA. Vital signs: Tobacco product use among middle and high school students – United States, 2011–2018. 2019. MMWR Morbidity Mortality Weekly Report. 68, 157–164. [PubMed: 30763302]
3. Halstead M, Gray N, Gonzalez-Jimenez N, Fresquez M, Valentin-Blasini L, Watson C, Pappas RS 2020. Analysis of Toxic Metals in Electronic Cigarette Aerosols Using a Novel Trap Design. Journal of Analytical Toxicology. 44, 149–155. [PubMed: 31588518]
4. Standard Reference Material 1898 Titanium Dioxide Nanopowder. National Institute for Standards and Technology. Gaithersburg, MD, USA. https://www-s.nist.gov/srmors/certificates/1898.pdf
5. CORESTA. 2015. Method Number 81. Routine analytical machine for e-cigarette aerosol generation and collection - definitions and standard conditions, CORESTA, Paris, France, pp. 1–6.
6. Pappas RS, Fresquez MR, Martone N, Watson CH 2014. Toxic metal concentrations in mainstream smoke from cigarettes available in the USA. Journal of Analytical Toxicology. 38, 204–211. [PubMed: 24535337]
7. Malvern Panalytical. https://www.materials-talks.com/blog/2014/08/05/faq-how-important-are-refractive-index-absorption-for-nanoparticles/
8. Malvern Panalytical. https://warwick.ac.uk/fac/cross_fac/sciencecity/programmes/internal/themes/am2/booking/particlesize/sample_dispersion__refractive_index_guide.pdf
9. Taylor JK 1987. Quality asssurance of chemical measurements. Lewis Publishers, Boca Raton, LA, pp. 79–81, 151–160.
10. Pace HE, Rogers NJ, Jarolimek C, Coleman VA, Higgins CP, Ranville JF 2011. Determining transport efficiency for the purpose of counting and sizing nanoparticles via single particle inductively coupled plasma mass spectrometry. Analytical Chemistry. 83, 9361–9369. [PubMed: 22074486]
11. Montaño MD, Olesik JW, Barber AG, Challis K, Ranville JF 2016. Single particle ICP-MS: Advances toward routine analysis of nanomaterials. Analytical and Bioanalytical Chemistry. 408, 5053–5074. [PubMed: 27334719]
12. Bihari P, Vippola M, Schultes S, Praetner M, Khandoga AG, Reichel CA, Coester C, Tuomi T, Rehburg M, Krombach F 2008. Optimized Dispersion of nanoparticles for biological *in vitro* and *in vivo* studies. Particle and Fiber Toxicology. 5, 14. DOI: 10.1186/1743-8977-5-14.
13. National Institute for Standards and Technology. Gaithersburg, MD, USA. https://nvlpubs.nist.gov/nistpubs/SpecialPublications/NIST.SP.1200-5r1.pdf
14. Malvern Panalytical. https://warwick.ac.uk/fac/cross_fac/sciencecity/programmes/internal/themes/am2/booking/particlesize/intro_to_dls.pdf
15. US Research. https://www.us-nano.com/inc/sdetail/55460 (last viewed 9 September 2019).
16. Tso C-P, Zhung C-M, Shih Y-H, Tseng Y-M, Wu S-C, Doong R-A 2010. Stability of metal oxide nanoparticles in aqueous solutions. Water Science & Technology. 61, 127–133. [PubMed: 20057098]

17. Gray N, Valentin-Blasini L, Watson CH, Pappas RS 2020. Toxic metals in liquid and aerosol from pod-type electronic cigarettes. Journal of Analytical Toxicology. 44, doi:
18. Wahlig H The differences between chromium & nickel stainless steel sinks. https://www.hunker.com/13402787/the-differences-between-chromium-nickel-stainless-steel-sinks Last viewed 23 September 2019.
19. International Stainless Steel Forum. The stainless steel family. http://www.worldstainless.org/Files/issf/non-image-files/PDF/TheStainlessSteelFamily.pdf Last viewed 23 September 2019.
20. Kamerud K, Hobbie KA, Anderson KA 2013. Journal of Agricultural and Food Chemistry. 61, 9495–9501. [PubMed: 23984718]
21. Chakravortty M, Paramguru RK, Jena PK 2001. Electrochemical dissolution of nichrome in sulphuric acid. Hydrometallurgy. 59, 45–54.
22. Farsalinos KE, Voudris V, Poulas K 2015. Are metals emitted from electronic cigarettes a reason for health concern? A risk-assessment analysis of currently available literature. International Journal of Environmental Research and Public Health. 12, 5215–5232. [PubMed: 25988311]
23. Hess CA, Olmedo P, Navas-Acien A, Goessler W, Cohen JE, Rule AM 2017. E-cigarettes as a source of toxic and potentially carcinogenic metals.152, 221–225.
24. Williams M, Bozhilov K, Ghai S, Talbot P 2017. Elements including metals in the atomizer and aerosol of disposable electronic cigarettes and electronic hookahs. PLoS One. 12(4): e0175430. [PubMed: 28414730]
25. Gray N, Halstead M, Gonzalez-Jimenez N, Valentin-Blasini L, Watson C, Pappas RS 2019. Analysis of toxic metals in liquid from electronic cigarettes. International Journal of Environmental Research and Public Health. 16: doi: 10.3390/ijerph16224450.
26. Pappas RS 2012. Toxic elements in tobacco and in cigarette smoke. (Annex 1) WHO Study Group on Product Regulation. WHO Technical Report Series 967, Geneva, Switzerland, pp 37–83.
27. Pappas RS 2011. Toxic elements in tobacco and in cigarette smoke: inflammation and sensitization. Metallomics. 3, 1181–1198. [PubMed: 21799956]
28. Zhang Q, Kusaka Y, Sato K Differences in the extent of inflammation caused by intratracheal exposure to three ultrafine metals: Role of free radicals. Journal of Toxicology and Environmental Health, A. 53, 423–438.
29. Gojova A, Guo B, Kota RS, Rutledge JC, Kennedy IM, Barakat AI 2007. Induction of inflammation in vascular endothelial cells by metal oxide nanoparticles: Effect of particle composition. Environmental Health Perspectives. 115, 403–409. [PubMed: 17431490]
30. Gower S, Hammond D 2007. CSP deposition to the alveolar region of the lung: Implications of cigarette design. Risk Analysis. 27, 1519–1533. [PubMed: 18093050]
31. Ferin J, Oberdörster G 1992. Translocation of particles from pulmonary alveoli into the interstitium. Journal of Aerosol Medicine. 5, 179–187.
32. Oberdörster G Oberdörster E Oberdörster J 2005. Nanotoxicology: An emerging discipline evolving from studies of ultrafine particles. Environmental Health Perspectives. 113, 823–839. [PubMed: 16002369]

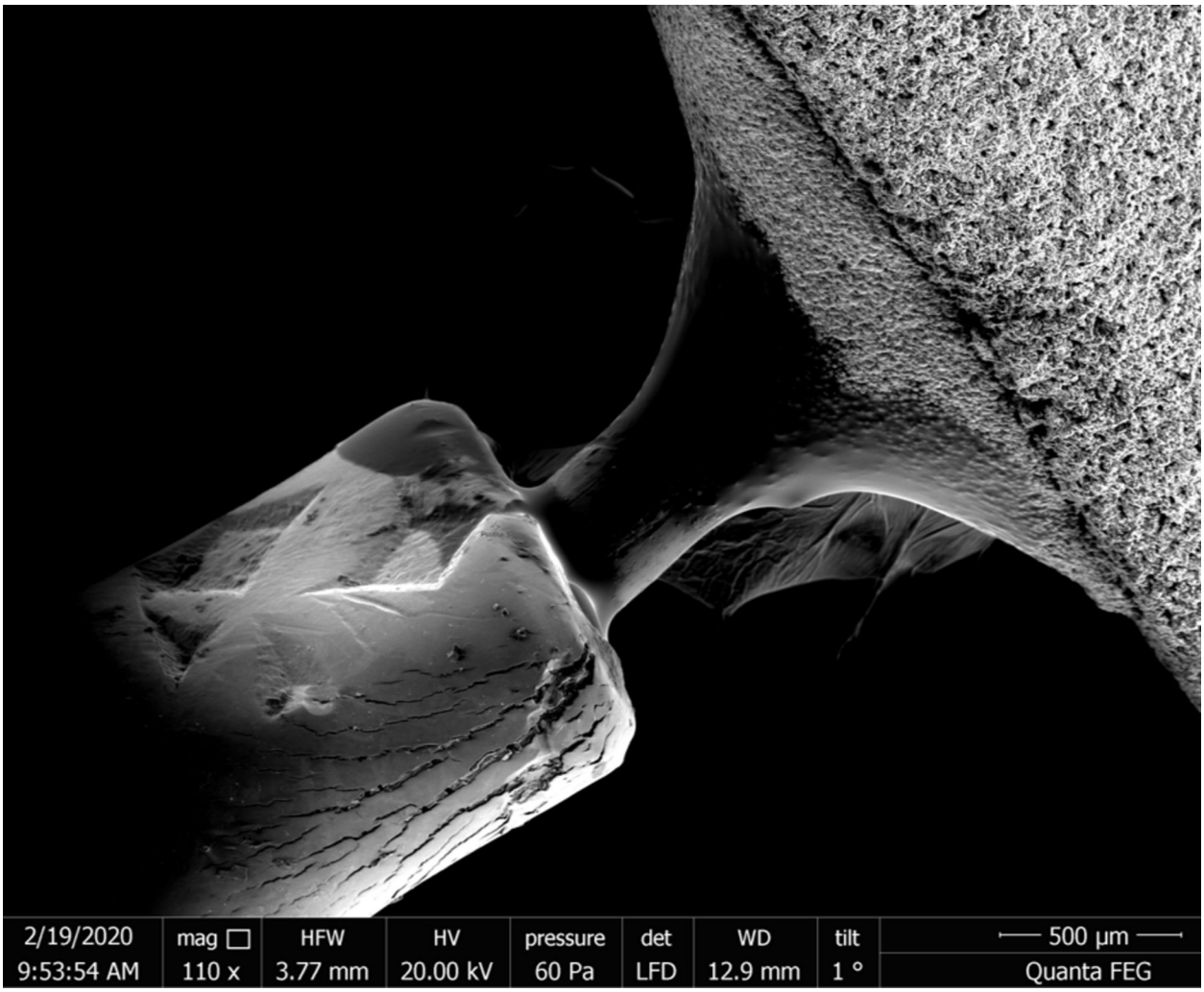

Figure 1.
Crimped connector from Vuse Alto® showing cracks in the connector surface that expose the substrate material beneath the coating alloy.

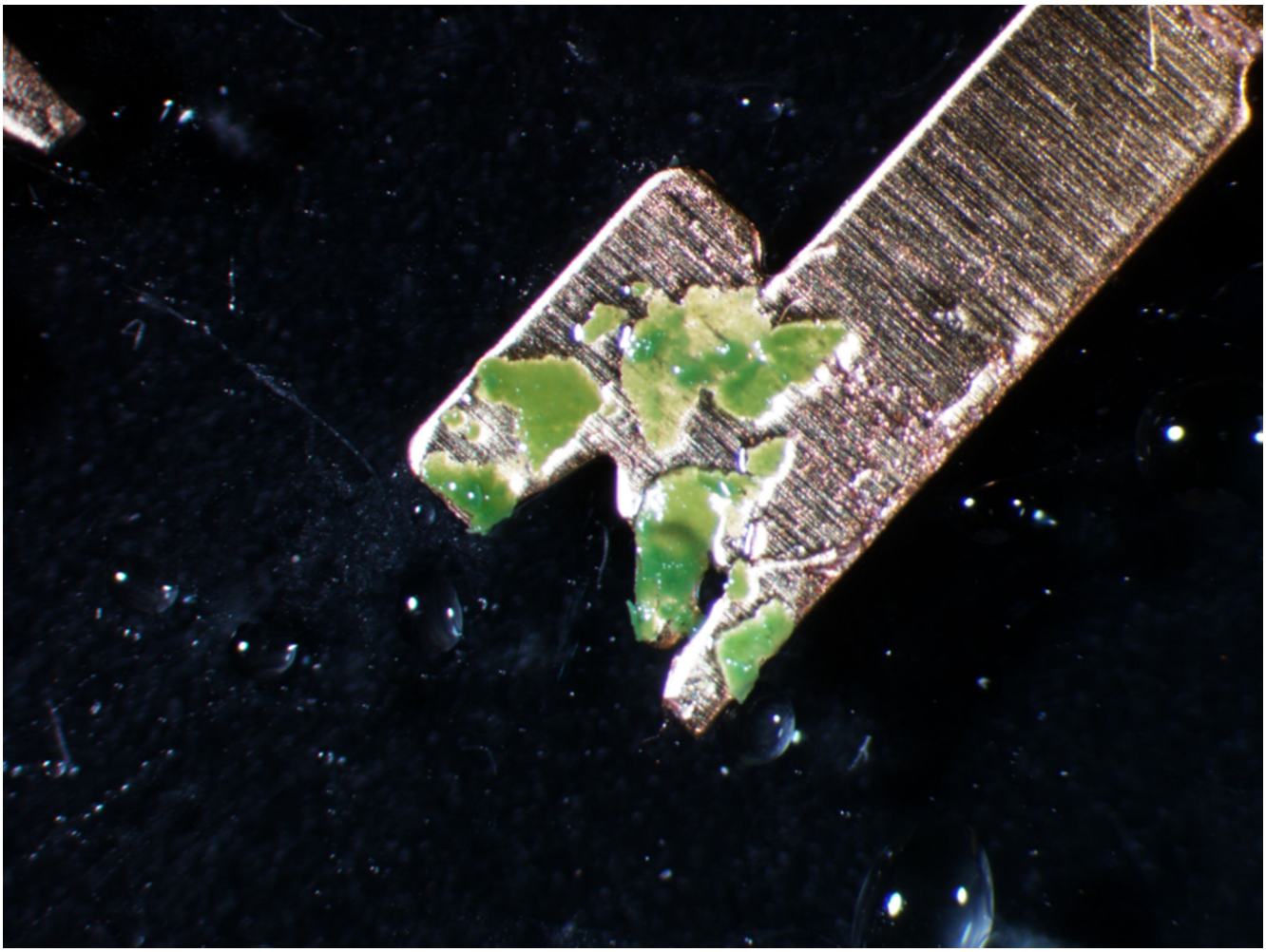

Figure 2.
Myblu® electrical connector showing oxidation or deposition of oxidized copper during vaping. Image was obtained using the microscope described in Materials and Methods.

Table 1.

Optimized settings for single and dual element particle analysis modes.

Single Element	NH_3 Flow (mL/min)	Axial Field Voltage	Dual Element	NH_3 Flow (mL/min)	Axial Field Voltage	Quadrupole Settle Time (μs)
^{197}Au	0	Not Applicable	^{118}Sn, ^{208}Pb	No Optimum Determined	No Optimum Determined	100
^{48}Ti	0	Not Applicable	^{52}Cr, ^{56}Fe	0.9	250	200
^{118}Sn	0	Not Applicable	^{52}Cr, ^{60}Ni	0.9	250	200
^{208}Pb	0	Not Applicable	^{56}Fe, ^{60}Ni	0.9	250	200
^{52}Cr	0.6	325	^{63}Cu, ^{66}Zn	0.5	250	200
^{63}Cu	0.7	325				
^{66}Zn	0.7	325				
^{60}Ni	1.0	325				
^{56}Fe	1.0	325				

Table 2.

Results of Nanocomposix 31 nm gold spheres stated size analyzed as samples at calculated 36,000 particles per mL dilution show acceptable size ranges and particle number concentrations. The particle size histogram was fairly symmetric, so most frequent and mean sizes were almost equivalent. *Particle number concentrations resulting from particle size calibration are frequently inaccurate in absence of an internal standard (11).

	Most Frequent Size (Per Cent Accuracy)	Mean Size (Per Cent Accuracy)	Particles/mL (Per Cent Accuracy)
Particle Concentration Calibration	33 ± 1 nm (105 ± 4%)	33 ± 2 nm (106 ± 6%)	36985 ± 4193 (103 ± 12%)
Particle Size Calibration	32 ± 2 nm (104 ± 5%)	33 ± 2 nm (105 ± 2%)	*

Table 3.

Results of NIST SRM 1898 titanium(IV) oxide nanopowder using SP-ICP-MS after sonication in ultrapure water show favorable particle size determination relative to other analytical techniques. DLS results were slightly higher than expected.

NIST SRM 1898 TiO_2 Results (nm)	CDC Results (nm): NIST TiO_2	NIST Certificate Laser Diffraction Spectrometry (nm)	NIST Certificate X-Ray Disk Centrifugation (nm)	NIST Certificate DLS (nm)
Most Frequent Size (SP-ICP-MS, Broad Asymmetric Peak)	37 ± 6	NA	NA	NA
Mean Size	77 ± 1	71 ± 4	77 ± 7	112 ± 4
Particle Size Detection Limit	17 ± 1	0.19 ± 0.05	NA	< 1.0
DLS Hydrodynamic Diameter (nm)	150 ± 11	NA	NA	112 ± 4

Table 4.

Manufactured nanopowder characteristics measured using SP-ICP-MS.

	Sonication Time Optimum (min)	Manufacturer Stated Size (nm)	Most Frequent Size (nm, RSD)	Mean Size (nm, RSD)	Particle Detection Limit (nm)
Cr_2O_3	30	60	60 ± 10 (17%)	103 ± 11 (11%)	15 ± 3
Fe_2O_3	30	20–40	23 ± 5	46 ± 7 (15%)	15 ± 2
Ni_2O_3	10	80	42 ± 19	50 ± 22 (44%)	28 ± 4
CuO	10	25–55	33 ± 7	70 ± 5 (7%)	15 ± 1
ZnO	1	35–45	68 ± 15	101 ± 28 (28%)	24 ± 1
SnO_2	10	35–55	35 ± 7	52 ± 2 (4%)	16 ± 1
Pb_2O_3	1	20–30	28 ± 12	42 ± 11 (26%)	14 ± 1

Table 5.

Results of particle analyses in aerosols from pod devices. NDP: No detectable particles, or indistinguishable from background. IT: Irregular Thresholds in multiple attempts prevented accurate particle counts at present stage of software development.

	Frequent Size (nm)	Mean Size (nm)	Particles per 10 Puffs (Range, nm)	Particle DL Mean (Range, nm)
Juul Mint® Cr	102 ± 9	103 ± 9	140 – 160	27
Juul Mint® Fe	41 ± 5	55 ± 8	6,200 – 13,000	16
Juul Mint® Ni	51 ± 6	66 ± 7	3,800 – 5,400	25
Juul Mint® Cu	27 ± 10	47 ± 34	2,000 – 20,000	15
Juul Mint® Zn	71 ± 19	85 ± 17	160 – 400	26
Juul Mint® Sn	24 ± 4	28 ± 4	72,00 – 21,000	14
Juul Mint® Pb	24 ± 9	35 ± 16	670 – 31,000	12
Juul Classic Tobacco® Cr	(0 – 61)	(0 – 123)	0 – 2,500	16
Juul Classic Tobacco® Fe	96 ± 34	184 ± 40	180 – 760	19
Juul Classic Tobacco® Ni	48 ± 18	57 ± 31	IT	32
Juul Classic Tobacco® Cu	31 ± 6	48 ± 18	1,600 – 53,000	18
Juul Classic Tobacco® Zn	NDP	NDP	NDP	28
Juul Classic Tobacco® Sn	25 ± 4	23 ± 5	IT	19
Juul Classic Tobacco® Pb	20 ± 3	20 ± 3	IT	14
myblu Mint-sation® Cr	0 – 81	0 – 82	0 – 162	26
myblu Mint-sation® Fe	99 ± 58	108 ± 50	130 – 810	22
myblu Mint-sation® Ni	136 ± 25	191 ± 20	490 – 1,500	33
myblu Mint-sation® Cu	281 ± 22	205 ± 23	19,000 – 84,000	(14 – 76)
myblu Mint-sation® Zn	NDP	NDP	NDP	23
myblu Mint-sation® Sn	92 ± 31	96 ± 29	160 – 1,800	(42 – 102)
myblu Mint-sation® Pb	NDP	NDP	NDP	17
myblu Tobacco Chill® Cr	37 ± 6	42 ± 10	3,500 – 13,000	17
myblu Tobacco Chill® Fe	76 ± 29	87 ± 27	3,500 – 16,000	(16 – 60)
myblu Tobacco Chill® Ni	55 ± 17	63 ± 22	IT	33
myblu Tobacco Chill® Cu	324 ± 32	271 ± 28	76,000 – 160,000	(34 – 83)
myblu Tobacco Chill® Zn	91 ± 28	99 ± 31	12,000 – 20,000	34
myblu Tobacco Chill® Sn	89 ± 12	111 ± 9	1,500 – 170,000	29
myblu Tobacco Chill® Pb	0 – 25	0 – 24	0 – 41,000	15
Vuse Alto Menthol® Cr	97 ± 10	113 ± 27	510 – 1,300	34
Vuse Alto Menthol® Fe	83 ± 3	105 ± 7	2,200 – 3,700	44
Vuse Alto Menthol® Ni	138 ± 23	163 ± 24	4,200 – 14,000	52
Vuse Alto Menthol® Cu	170 ± 78	197 ± 49	26,000 – 160,000	25

	Frequent Size (nm)	Mean Size (nm)	Particles per 10 Puffs (Range, nm)	Particle DL Mean (Range, nm)
Vuse Alto Menthol® Zn	0 – 302	0 – 259	0 – 1,500	(62 – 354)
Vuse Alto Menthol® Sn	59 ± 18	68 ± 15	3,600 – 5,000	28
Vuse Alto Menthol® Pb	80 ± 21	90 ± 16	16,000 – 26,000	(54 – 181)
Vuse Alto Rich Tobacco® Cr	57 ± 11	88 ± 17	540 – 2,400	18
Vuse Alto Rich Tobacco® Fe	70 ± 7	109 ± 15	970 – 1,600	23
Vuse Alto Rich Tobacco® Ni	76 ± 46	74 ± 40	630 – 190,000	34
Vuse Alto Rich Tobacco® Cu	77 ± 24	138 ± 34	2,400 – 12,000	20
Vuse Alto Rich Tobacco® Zn	119 ± 20	132 ± 22	200 – 13,000	(31 – 61)
Vuse Alto Rich Tobacco® Sn	37 ± 8	43 ± 10	14,000 – 19,000	20
Vuse Alto Rich Tobacco® Pb	45 ± 18	47 ± 19	9,700 – 222,000	23

Table 6.

Results of dual element particle analyses in aerosols from mint or menthol flavored pod devices. IT: Irregular thresholds were repeatedly encountered during analyses of aerosols obtained from these pods preventing accurate analyses.

Pod, Flavor	Paired Element Particles
Juul Mint® Cr/Fe	Cr: 100%, Fe: 4.2%
myblu Mint-Sation® Cr/Fe	Cr: 50%, Fe: 10%
Vuse Alto Menthol® Cr/Fe	Cr: 0%, Fe: 0%
Juul Mint® Cr/Ni	Cr: 20%, Ni: 2.0%
myblu Mint-Sation® Cr/Ni	Cr: 0%, Ni: 0%
Vuse Alto Menthol® Cr/Ni	Cr: 0%, Ni: 0%
Juul Mint® Fe/Ni	Fe: 49%, Ni: 19%
myblu Mint-Sation® Fe/Ni	Fe: 0%, Ni: 0%
Vuse Alto Menthol® Fe/Ni	Fe: 16%, Ni: 5.8%
Juul Mint® Cu/Zn	IT
myblu Mint-Sation® Cu/Zn	IT
Vuse Alto Menthol® Cu/Zn	Cu: 0.5%, Zn: 43%

Table 7.

Results of dynamic light scattering analyses of particles in aerosols as copper(II) oxide.

	Principal Peak (nm)	Frequent Size from Table 5 (nm)
Juul Classic Tobacco®	173 ± 46	31 ± 6
Vuse Alto Rich Tobacco®	87 ± 30	77 ± 24
myblu Tobacco Chill®	252 ± 119	324 ± 32
Juul Mint®	161 ± 26	27 ± 10
Vuse Alto Menthol®	130 ± 33	170 ± 78
myblu Mint-sation®	248 ± 125	281 ± 22